CERN-ATS-Note-2012-074 MD

24 September 2012
Gianluca.Valentino@cern.ch
Stancari@fnal.gov

Halo Scraping, Diffusion and Repopulation MD

G. Valentino, R. W. Assmann, R. Bruce, F. Burkart, S. Redaelli,
B. Salvachua, CERN, Geneva, Switzerland
V. Previtali, G. Stancari, A. Valishev, Fermilab, Batavia, IL, USA

Keywords: LHC beam scraping, diffusion, halo repopulation

Summary

Beam halo measurements in the LHC were conducted through collimator scrapings in an MD carried out on the 22nd June 2012 for the first time at 4 TeV. The time evolution of losses during a collimator scan provides information on halo diffusion and population. Four scans were performed with two collimators in the vertical and horizontal plane in B1 and B2 respectively, before and after bringing the beams into collisions. During an inward step, the beam losses measured at the BLMs for the first 3 seconds are believed to be dominated by multi-turn halo removal by the collimator jaw. However, a good comparison was found between fits of the diffusion model and the subsequent loss decay. In addition, the fitted diffusion coefficients compare well to the coefficients estimated from the core emittance growth rates as a function of action.

1 Introduction

Understanding particle losses and beam quality degradation is one of the fundamental aspects in the design and operation of accelerators. The dynamics of particles in an accelerator can be quite complex. Deviation from linear dynamics can be large, especially in the beam halo. Lattice resonances and non-linearities, coupling, intrabeam and beam-gas scattering, as well as the beam-beam force in colliders all contribute to the topology of the particles' phase space, which in general will include regular and chaotic regions, and resonant islands. In addition, various noise sources are present in a real machine, such as ground motion (resulting in orbit and tune jitter) and ripple in the radio-frequency and magnet power supplies. As a result, the macroscopic motion can acquire a stochastic character, which can be described in terms of particle diffusion [1–5].

The LHC collimators are arranged in a four-stage hierarchy to scatter and absorb beam halo particles before they are deposited in the super-conducting magnets, which may cause quenches. Apart from serving to protect the machine, they may also be used as diagnostic tools, for example to measure the local beam center and beam size. The time evolution of

losses during a collimator scan gives information on halo diffusion, halo population, emittance growth, beam lifetime and collimation efficiency as a function of collimator position. This study is also useful to check calculations of the dynamic aperture, and augments the experimental understanding of present and future collimation systems: how fast particles get to the collimators, how many of them etc. A model capable of predicting the BLM signal spike and the corresponding temporal decay would be an input to establish new algorithms aimed at improving the collimator alignment procedure [6].

A complete set of slow beam scrapings was performed in the LHC for the first time in 2011 at 450 GeV [7]. The measurement data was fitted with a double Gaussian function, and the conclusions of this study were that the horizontal tails are more populated than the vertical tails. An MD request for scraping at 4 TeV was made for 2012 following the development of a diffusion model based on Tevatron data [8]. The aim of the study is to develop a model based on diffusion to predict the beam losses before, during and after a collimator step, both inward and outward. These measurements profited from the new 12.5 Hz BLM data, whereas only 1 Hz data was available in the 2011 MD. The measurements were done with squeezed separated and colliding beams to assess beam-beam effects on diffusion.

2 Diffusion Model

Particle motion at the microscopic level is in general very complex. Two main considerations lead to the *ansatz* that macroscopic motion in a real machine, especially in the halo, will be mostly stochastic: (1) the central limit theorem applied to the multitude of dynamical effects acting on the beam; (2) the operational experience during collimator setup, which generates loss spikes and loss dips which often decay in time as $1/\sqrt{t}$.

A diffusion model of the time evolution of loss rates caused by a collimator jaw step was developed in [9]. It builds upon the model of Ref. [10] and its assumptions: (1) constant diffusion rate within the range of the step and (2) linear halo tails. These hypotheses allow one to obtain analytical expressions for the solutions of the diffusion equation and for the corresponding loss rates as a function of time. The model in [9] addresses some of the limitations of the previous model and expands it in the following ways:

1. losses before, during, and after the step are predicted;
2. different steady-state rates before and after are explained;
3. determination of the model parameters (diffusion coefficient, tail population, detector calibration and background rate) is more robust and precise.

These calculations are the basis for the measurement of transverse beam diffusion rates as a function of particle amplitude with collimator scans. The derivation of the loss evolution equations is presented in [9]. The loss rate evolution measured by the BLMs can be expressed in terms of the particle loss rate L, a normalization constant k and a background term B:

$$S = kL + B \tag{1}$$

The particle loss rate at the collimator is in turn given by the product of the diffusion coefficient D and the partial derivative of the phase-space density with respect to action:

$$L = -D \times [\partial_J f]_{J=J_c} \tag{2}$$

The value of the gradient at the collimator for an inward step is therefore:

$$\partial_J f_I(J_c, t) = -A_i + 2(A_i - A_c)P(\frac{-J_c}{\sigma}) + \frac{1}{\sqrt{2\pi}\sigma}\{-2A_i(J_{ci} - J_c) + 2(A_i J_{ci} - A_c J_c)e^{[-\frac{1}{2}(\frac{J_c}{\sigma})^2]}\} \tag{3}$$

and correspondingly for an outward step:

$$\partial_J f_O(J_c, t) = -2A_i P(\frac{J_{ci} - J_c}{\sigma}) + 2(A_i - A_c)P(\frac{-J_c}{\sigma}) + 2\frac{A_i J_{ci} - A_c J_c}{\sqrt{2\pi}\sigma}e^{[-\frac{1}{2}(\frac{J_c}{\sigma})^2]} \tag{4}$$

where σ is a term that includes the diffusion coefficient and varies with time t:

$$\sigma = \sqrt{2Dt} \tag{5}$$

3 MD Experimental Procedure

3.1 Beam Parameters and Machine Configuration

The MD beam parameters, including the beam energy and the starting intensity for each scraping configuration are shown in Table 1. One nominal bunch (1.15×10^{11} p) per beam was used.

Table 1: The MD beam parameters at the start of both scraping configurations.

Parameter	Separated Beams	Colliding Beams
Energy [GeV]	4000	4000
Intensity B1 [p]	1.291×10^{11}	1.143E11
Intensity B2 [p]	1.072×10^{11}	0.740E11
β^* IP1/5 [cm]	60	60
β^* IP2/8 [cm]	300	300

3.2 MD Programme

The study started off with squeezed, non-colliding beams at an energy of 4 TeV. The IR7 primary and secondary collimators were retracted from their nominal settings of 4.3 σ and 6.3 σ from the beam center respectively to a half gap of 7 σ, in order to have a larger scan range. The beam centers at these collimators were measured during beam-based alignment in March 2012, and are used throughout the 2012 LHC run. The 1 σ beam size is determined from the nominal beam emittance and local beta functions at the individual collimators. An overview of the settings of the collimators not used for scraping during the MD are shown in Table 2. The settings for these collimators are the same which are used in normal operation, bar the IR7 TCPs and TCSGs.

Table 2: The settings of the collimators not used for scraping throughout the MD (grouped by families), for both scraping configurations.

Collimator Family	Half Gap [σ]
TCP IR3	12
TCSG IR3	15.6
TCLA IR3	17.6
TCP IR7	7
TCSG IR7	7
TCLA IR7	8.3
TCSG IR6	7.1
TCDQ IR6	7.6
TCT IR1/5	9
TCT IR2/8	12
TCL	out

In the study, the left jaws of the TCP.D6L7.B1 (vertical plane) and the TCP.C6R7.B2 (horizontal plane) collimators were moved in steps of 5 μm to 20 μm. The collimators were selected from different beams to be able to perform the scrapings in parallel without inducing cross-talk in the BLM signals. The jaws were moved in as soon as the beam losses from the previous step had decayed back to a steady-state (approximately every 10 to 40 seconds).

The jaws were left for a few minutes in the beam after they had reached their final inward position, to allow the losses to stabilize. Subsequently, the jaws were moved out in steps of 20 μm to 100 μm, with the next step being taken when a steady-state loss rate was observed. The beams were then brought into collisions, and the procedure was repeated. The initial and final jaw positions for each scraping in terms of the nominal beam size are provided in Table 3.

Table 3: The initial and final collimator jaw nominal half gaps in units of σ for the different scrapings. The beam centers determined in beam-based alignments in March 2012 and used during operation are assumed for the calculation.

Collimator	**Separated Beams**	**Colliding Beams**
TCP.D6L7.B1 (initial)	7.00 σ	7.00 σ
TCP.D6L7.B1 (final)	1.96 σ	2.41 σ
TCP.C6R7.B2 (initial)	7.00 σ	7.00 σ
TCP.C6R7.B2 (final)	1.76 σ	2.31 σ

3.3 Measured Variables

The halo diffusion model depends on beam intensities, emittances, bunch length and momentum spread. The collimator positions and local losses need to be accurately recorded. The measured variables are the following:

- **Intensity:** The fast beam current transformer data (FBCT) is logged at a rate of 1 Hz. The data was also logged every 20 ms.
- **Wire-scan emittances:** Three sets of wire scans were taken: (1) squeezed beams, before scraping; (2) squeezed beams, after scraping; (3) colliding beams before scraping. Some measurements may not be accurate due to saturation.
- **Synchrotron-light emittances:** Synchrotron-light emittance measurements (BSRT) were logged continuously every 3 seconds.
- **Bunch length:** Profiles from the longitudinal density monitor (LDM) for both beams were taken at flat top and after scraping with squeezed beams. The data files include the sampled data for a full turn (89 μs) every 25 ps. The r.m.s. bunch length is about 0.3 ns. Satellite bunches are present but are most likely negligible for the purposes of the study.
- **Momentum spread:** Estimates of the momentum spread can be obtained from the longitudinal profile and from the parameters of the accelerating cavities.
- **Collimator positions:** The left and right collimator jaw positions are logged at a rate of 1 Hz. The jaws were kept to the zero angle throughout the study. The plots in Fig. 1 show the beam intensity and positions of the IR7 primary collimators used for scraping throughout the MD.
- **Beam losses:** The BLM data was acquired at a rate of 1 Hz (1.3 s integration time) and 12.5 Hz (82 ms integration time). The typical background signal is 2×10^{-7} Gy/s, with a noise of 10^{-8} Gy/s. The signal varies from 10^{-7} Gy/s to 10^{-3} Gy/s (close to the beam dump threshold), as the collimator jaw cuts deeper into the beam halo.

4 Data Analysis

The variation in the BLM signals normally used for collimator analysis and the collimator jaw positions throughout the MD are shown in Fig. 2 for the two scraping tests done for each beam. A zoom into all plots for the last few inward steps and the outward steps is given in Fig. 3. A comparison of the responses of the first 4 BLMs immediately downstream of the collimator of interest is shown in Fig. 4. As expected, similar loss profiles with different offsets are observed for the different monitors.

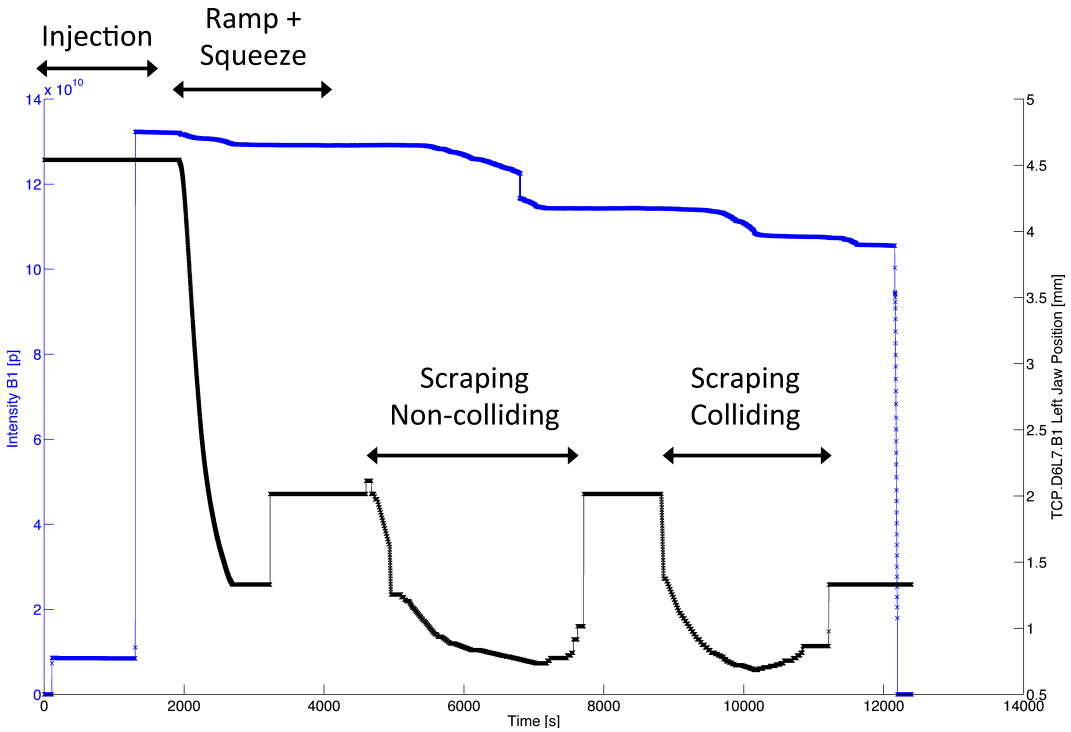

(a) Beam intensity and TCP.D6L7.B1 left jaw positions for B1

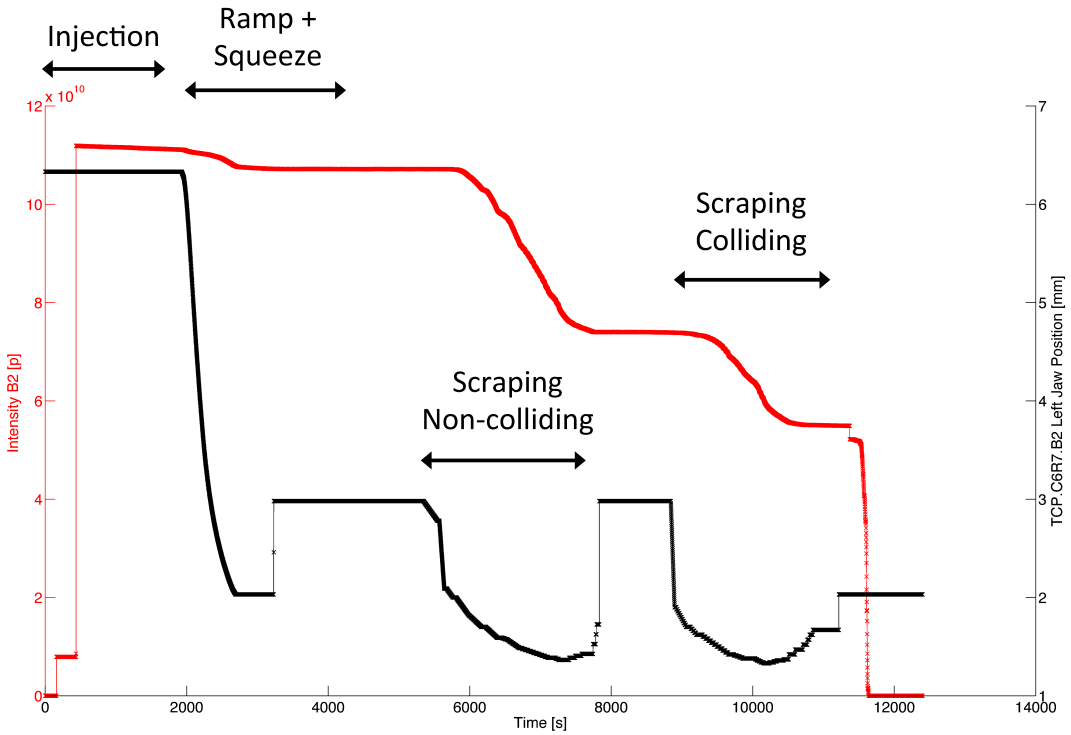

(b) Beam intensity and TCP.C6R7.B2 left jaw positions for B2

Figure 1: The beam intensities and the collimator positions as a function of time (t[0] = 22.06.2012 04:30:00). Scraping with the left jaws of the TCP.D6L7.B1 (vertical plane) and TCP.C6R7.B2 (horizontal plane) was performed with squeezed non-colliding and colliding beams.

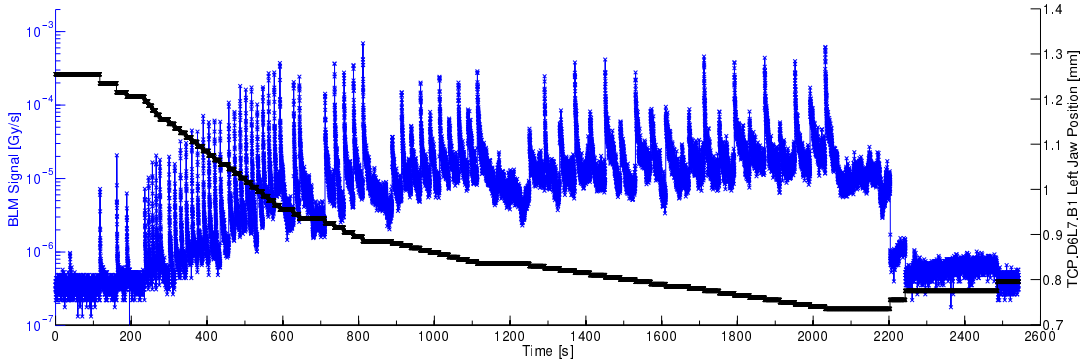

(a) BLM signal and TCP.D6L7.B1 left jaw positions for B1 (separated beams).

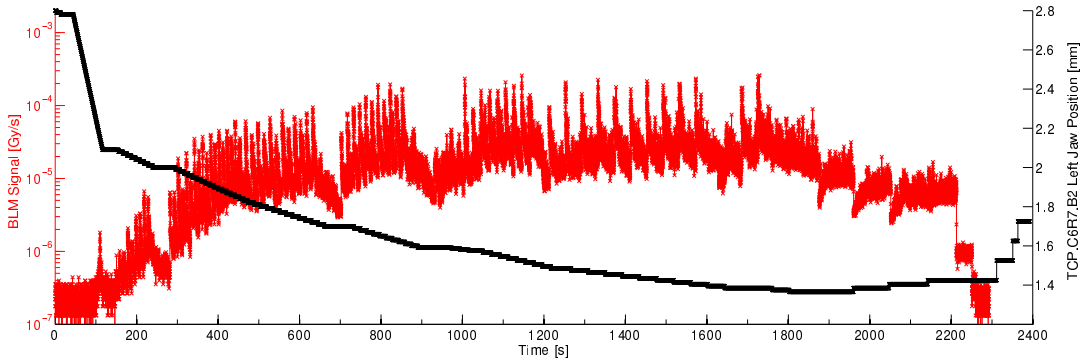

(b) BLM signal and TCP.C6R7.B2 left jaw positions for B2 (separated beams).

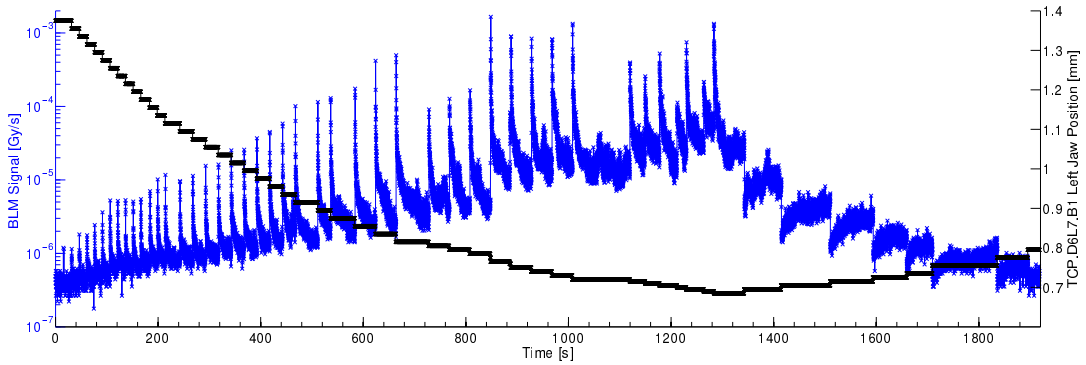

(c) BLM signal and TCP.D6L7.B1 left jaw positions for B1 (colliding beams).

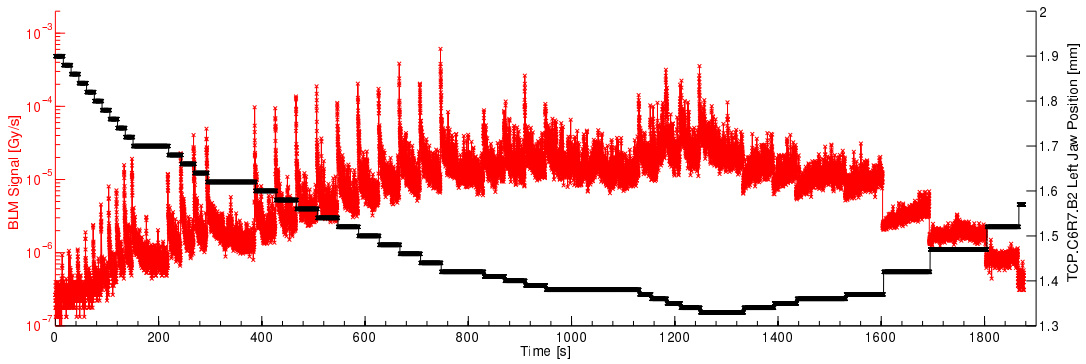

(d) BLM signal and TCP.C6R7.B2 left jaw positions for B2 (colliding beams).

Figure 2: The collimator positions and the associated BLM signals as a function of time with separated beams (t[0] = 22.06.2012 06:00:00) and colliding beams (t[0] = 22.06.2012 07:00:00).

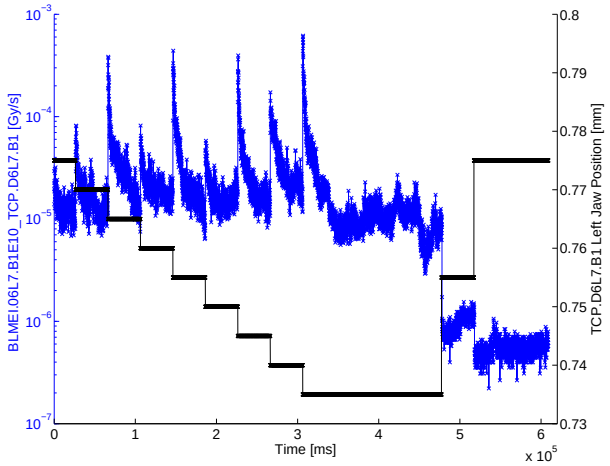

(a) BLM signal and TCP.D6L7.B1 left jaw positions

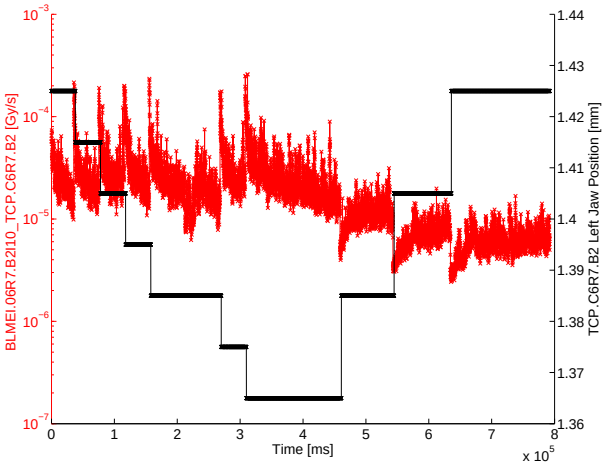

(b) BLM signal and TCP.C6R7.B2 left jaw positions

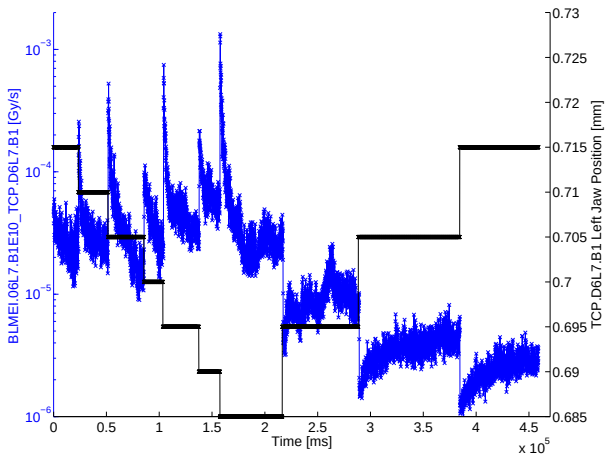

(c) BLM signal and TCP.D6L7.B1 left jaw positions

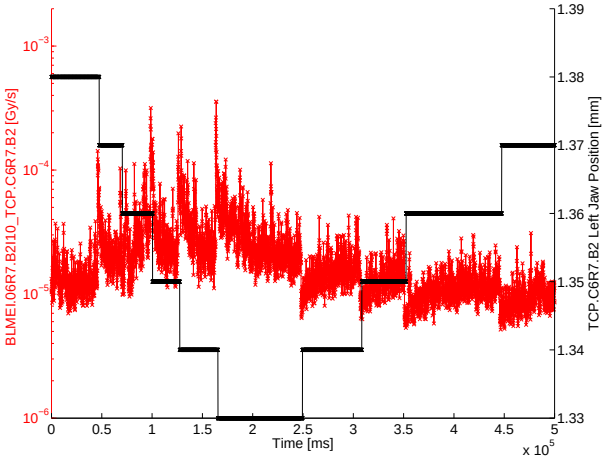

(d) BLM signal and TCP.C6R7.B2 left jaw positions

Figure 3: Zoom in the BLM signals and the collimator positions as a function of time, to illustrated the loss behaviour with inward and outward steps.

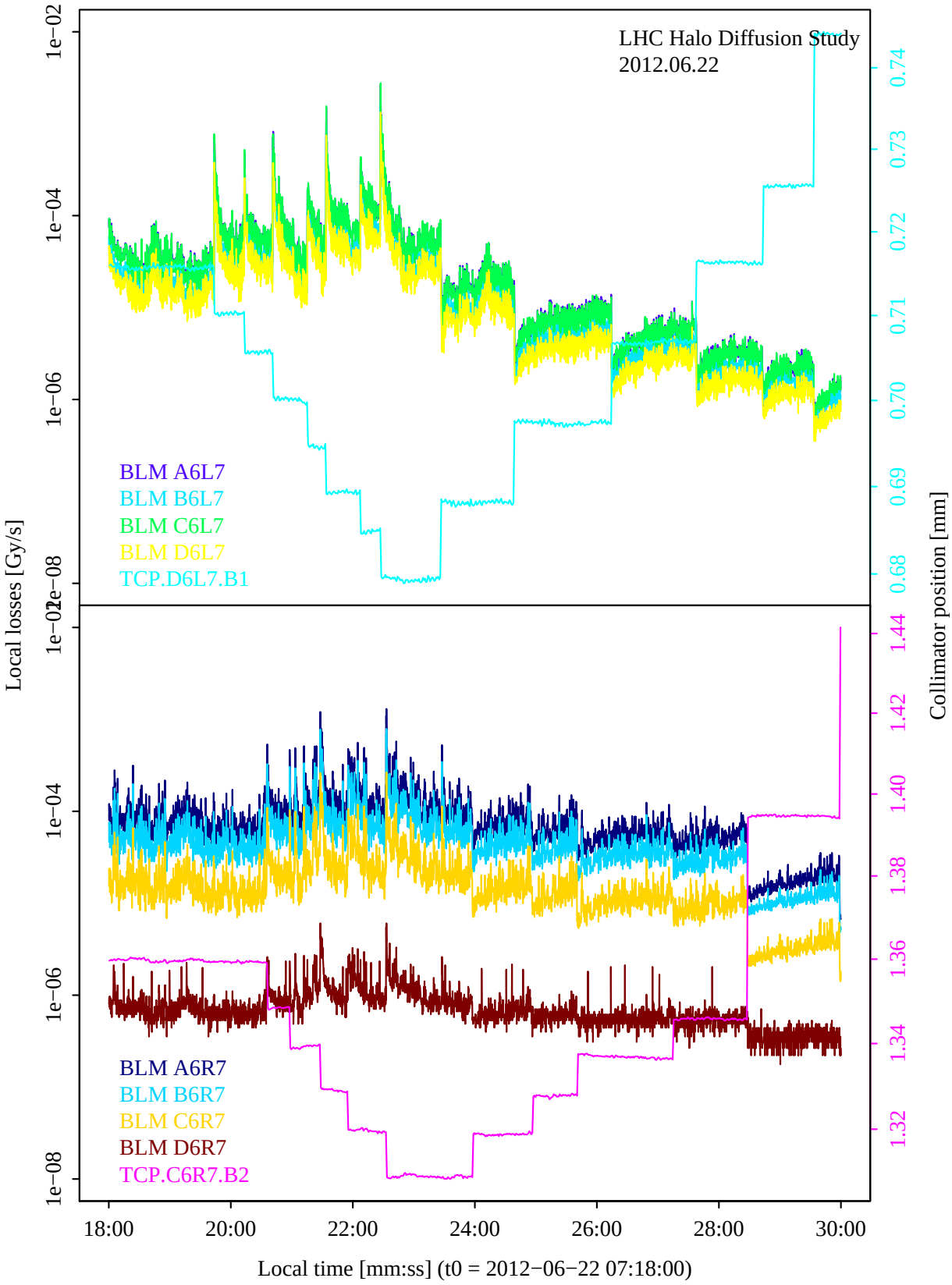

Figure 4: Comparison of local loss monitors for a portion of the collimator scan.

4.1 BCT-BLM calibration

There are approximately 3600 BLM ionization chambers installed around the LHC, which measure beam losses in Gy/s. However, it is useful to also be able to measure the losses in terms of protons. Calibration factors which allow conversion from beam loss in Gy/s to p/s would be useful in determining the beam lifetime and evaluating the performance of the machine. The background losses (the B parameter in Eq. (1)) are determined during "quiet time", with no beam in the machine (between 2012-06-22 05:28:00 and 2012-06-22 05:48:00). For the local B1 BLMs the background level is 1.81×10^{-6} Gy/s, and 1.06×10^{-6} Gy/s for B2.

For calibrating the response of this group of BLMs (conversion from Gy/s to protons/s), the experiment time is subdivided into 20-second intervals (40 μm groupings of the collimator half gap) to obtain the average collimator position, local loss rate and intensity decay rate. The 20-second period was chosen to obtain a better resolution in the intensity decrease, as for some individual loss spikes (particularly at a larger half gap) the intensity decrease is not discernible. The BLM loss rate as a function of the total particle loss rate is shown in Fig. 5. As expected, there is a systematic shift between separated and colliding beams in the total loss rate (all BLMs around the ring), due to luminosity losses. The local losses (the closest 4 BLMs downstream of the collimator) appear to scale linearly with proton losses when the collimator of interest is the leading jaw.

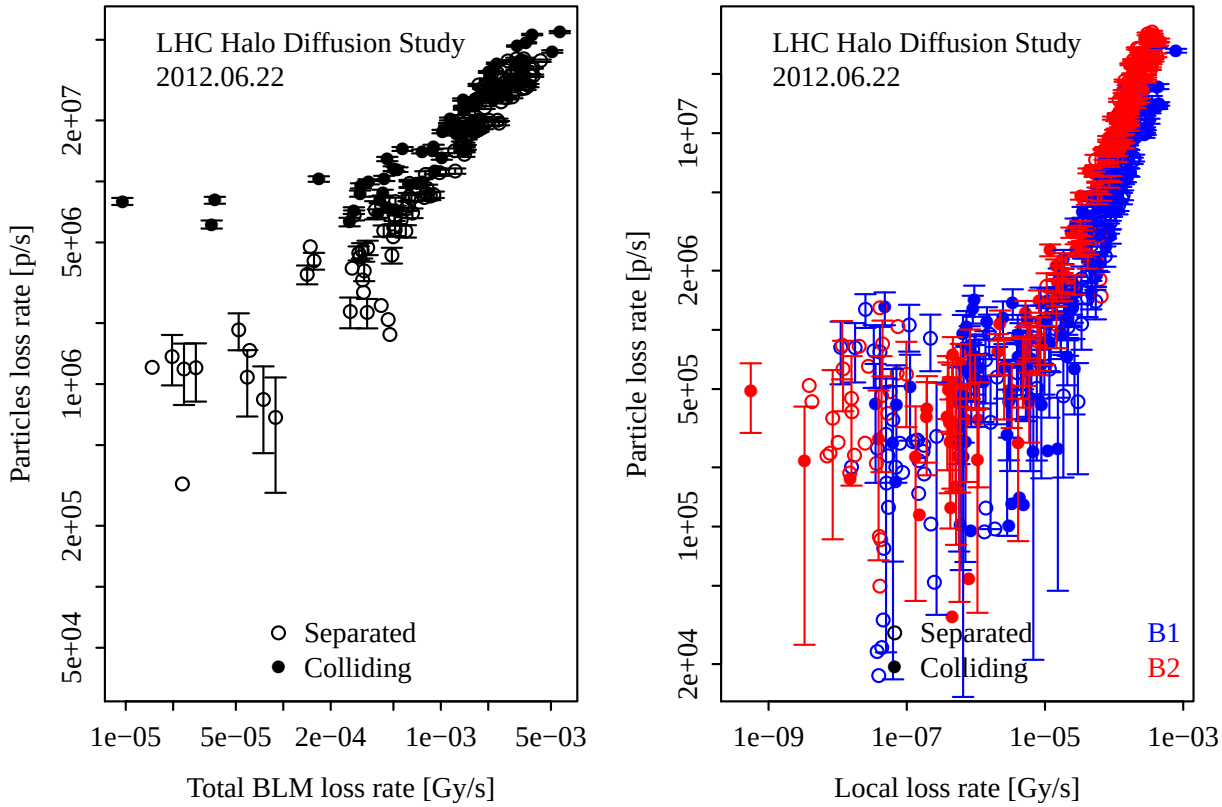

Figure 5: Particle loss rates vs. BLM loss rates: total (all BLMs, both beams) on the left; divided by beam (only local primary BLMs) on the right.

Figure 6 shows the variation of the BLM calibration constant as a function of the collimator half gap. The calibration factor, or "local loss detection efficiency", varies by more than 2 orders of magnitude. It clearly exposes the threshold when the collimator becomes the leading edge - a half gap of 0.8 mm in the vertical plane and 1.5 mm horizontally. As expected, the efficiency in collisions is lower, when a larger beam fraction is lost at the experimental insertion points. This is particularly obvious in the horizontal case. For the purposes of the diffusion analysis, these numbers are an experimental measurement of the k parameter in Eq. (1). In Fig. 6, the measurements of k as a function of collimator position are interpolated with a smooth spline with 4 degrees of freedom.

The dose-intensity calibration factors were also obtained using the information on the BLM spikes over intervals of 1 s from the jaw movement, with the BLM taken to be the one downstream closest to the collimator. The advantage in this case is that any intensity decrease can be directly correlated to the loss spike under study. The BLM and intensity data were extracted for each loss spike interval. The dose in Gy was calculated as the average loss signal for the peak integrated over ∼1 s, as shown in Fig. 7(a) and Fig. 7(c). The intensity lost over the same time period was also determined (see examples in Fig. 7(b)

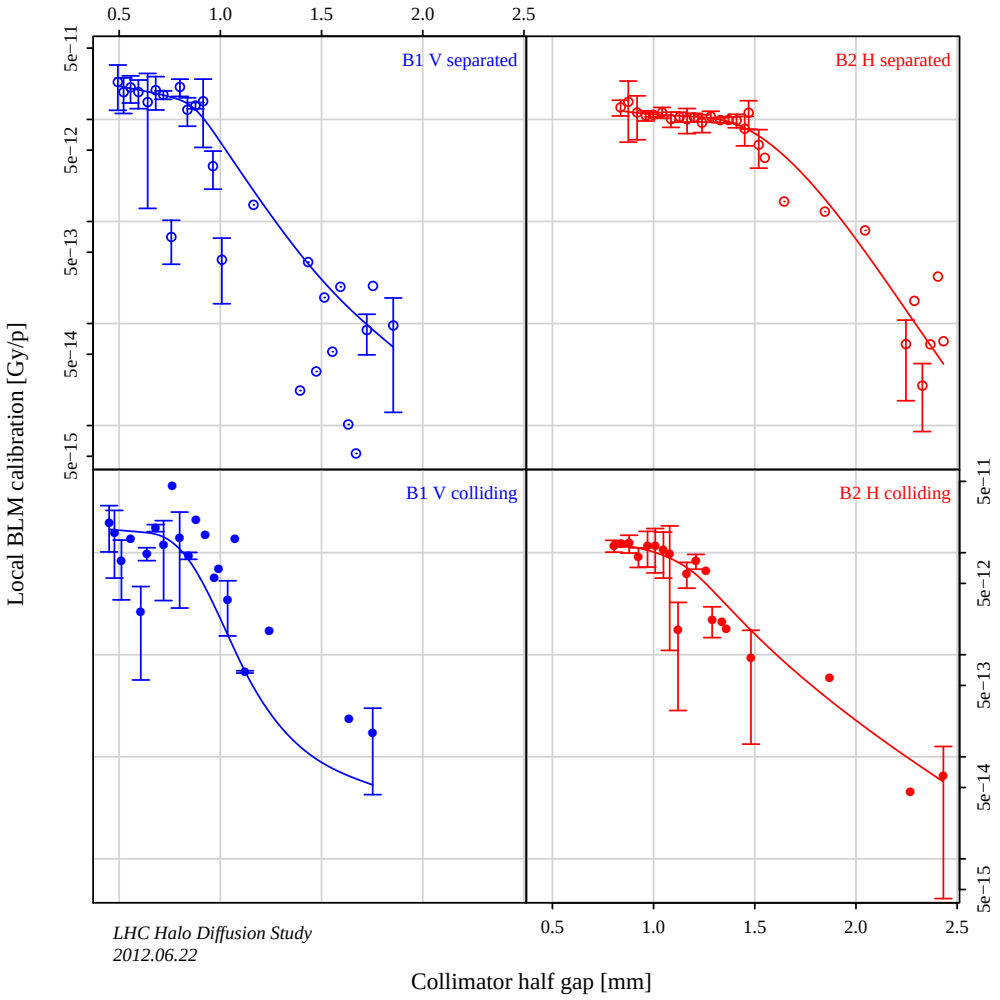

Figure 6: Local loss monitor calibration vs. collimator position.

and Fig. 7(d)). The particle loss was calculated as a percentage of the intensity recorded by the FBCT before the loss spike, and is shown as a function of the jaw gap in mm in Fig. 8(a) and 8(b).

The calibration factors in p/Gy and Gy/p are shown in Fig. 9(a) and Fig. 9(b). The values compare well with those found during the 2011 scraping MD for the same collimators (1.2×10^{12} p/Gy, see [7,11]). Note that the apparent difference in scale between Fig. 9(a) and Fig. 6 is because the former plot takes into account only the closest BLM to the collimator, while the latter considers the four closest downstream BLMs. The theoretical particle loss

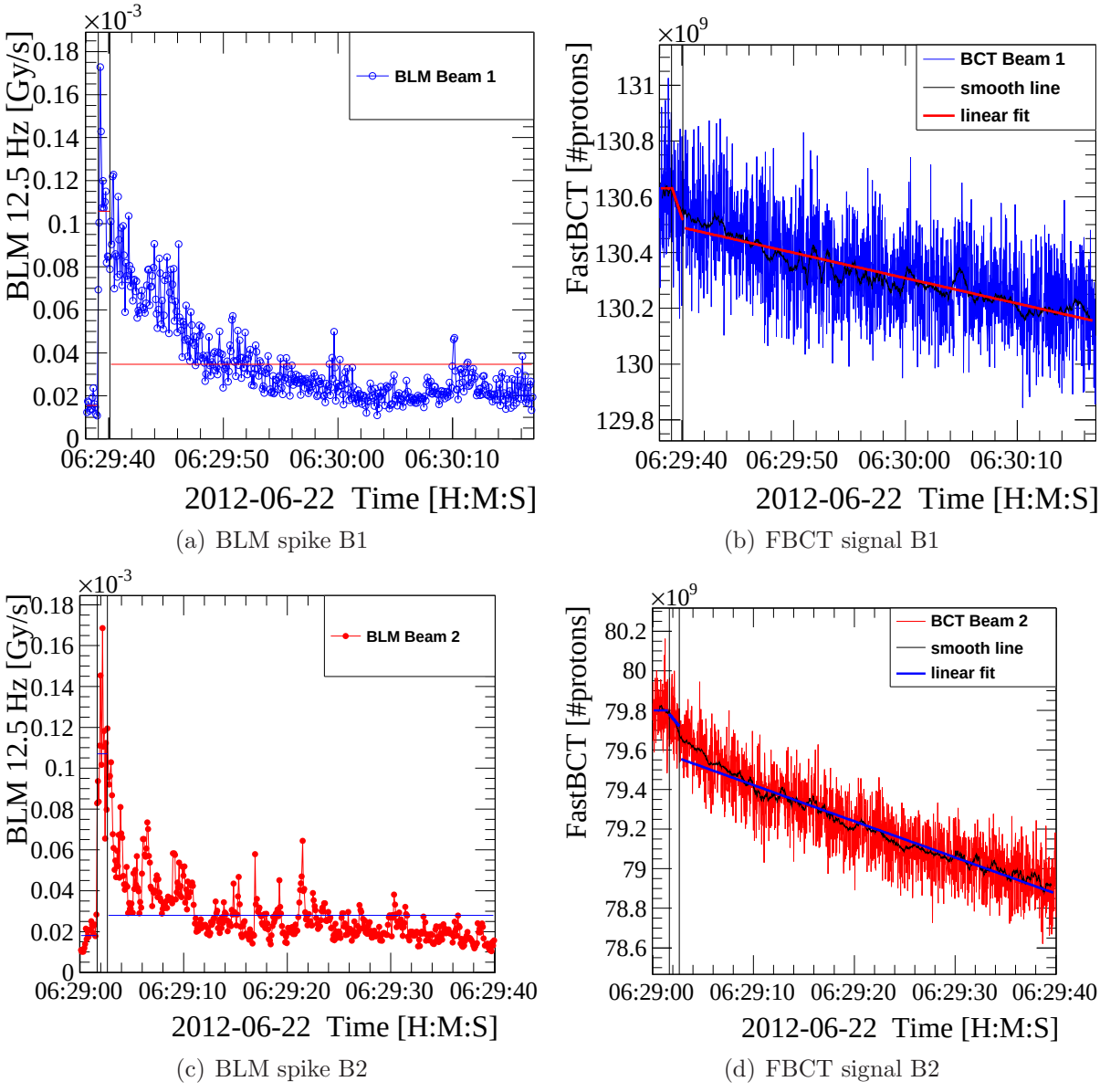

(a) BLM spike B1

(b) FBCT signal B1

(c) BLM spike B2

(d) FBCT signal B2

Figure 7: Examples of fits made to the BLM and FBCT signals during loss spikes following a B1 (top) and B2 (bottom) collimator jaw movement respectively. The dose in Gy is calculated by integrating the BLM signal over ∼1 s and the intensity lost in the same period is determined to calculate the calibration factor for each loss spike.

was calculated for a given jaw half gap by integrating over the Gaussian beam distribution for the jaw step size used. Figures 8(c) and 8(d) shows the BLM signal in arbitrary units, which is calculated by multiplying the ratio of the dose to the intensity before the jaw movement by the average calibration factor of 1.2×10^{12} p/Gy and an additional factor. The additional factor ($\sim$0.65) was necessary to scale the resulting BLM signal to the theoretical curves, which are the same as in Figs. 8(a) and 8(b), and derives from an offset between the FBCT signal and the actual intensity in the LHC. The discontinuities in the theoretical curves are due to different jaw step sizes being used throughout the MD.

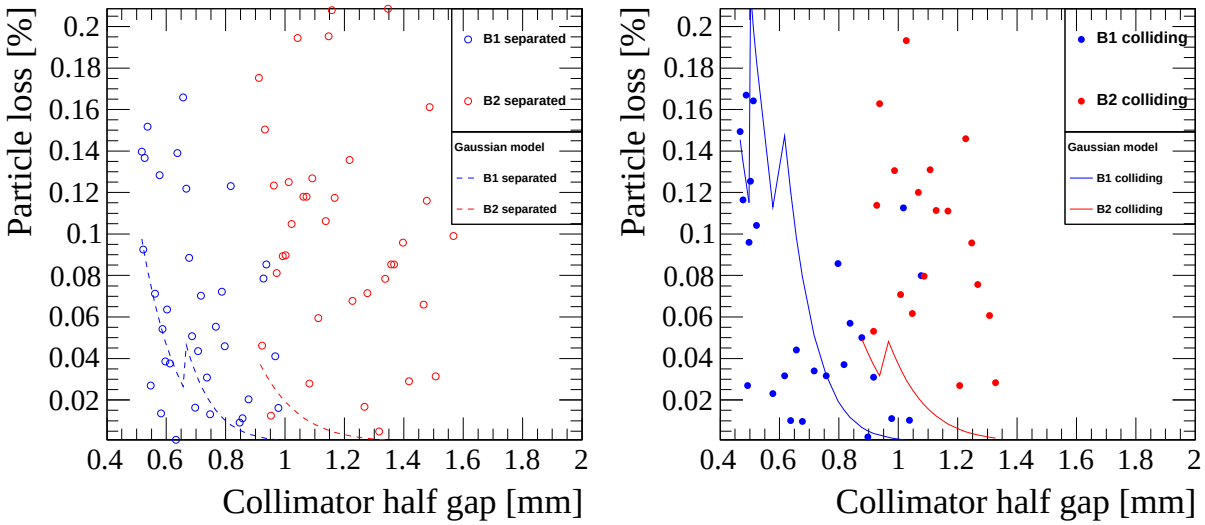

(a) Particle loss (separated beams)

(b) Particle loss (colliding beams)

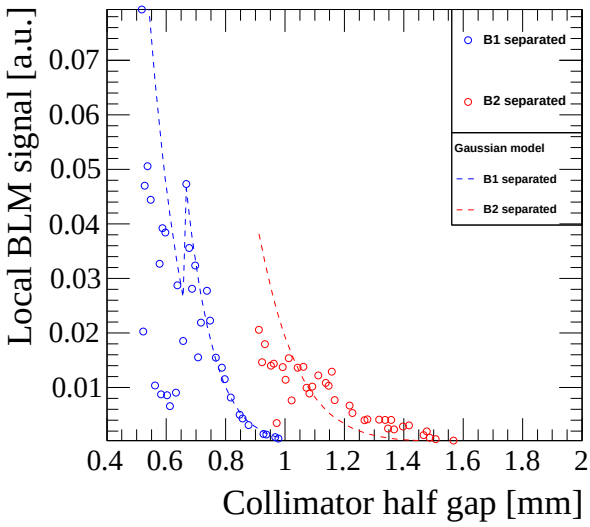

(c) Local BLM signal (separated beams)

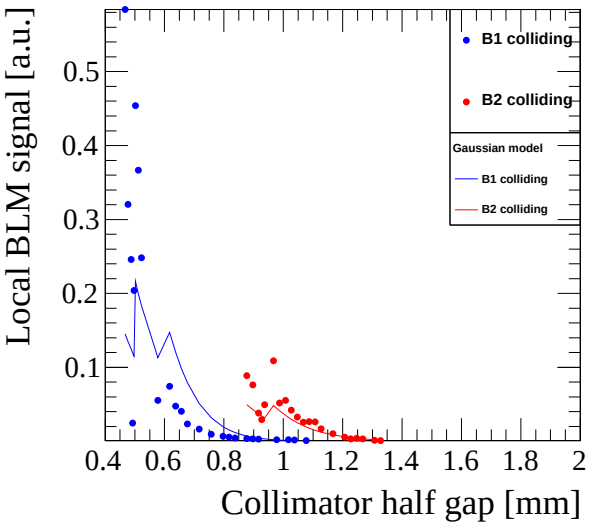

(d) Local BLM signal (colliding beams)

Figure 8: Particle loss as a percentage of the intensity measured before the loss spike (top) and local BLM signal (bottom), with comparison to the theoretical values. The discontinuities in the theoretical curves are due to different jaw step sizes being used throughout the MD.

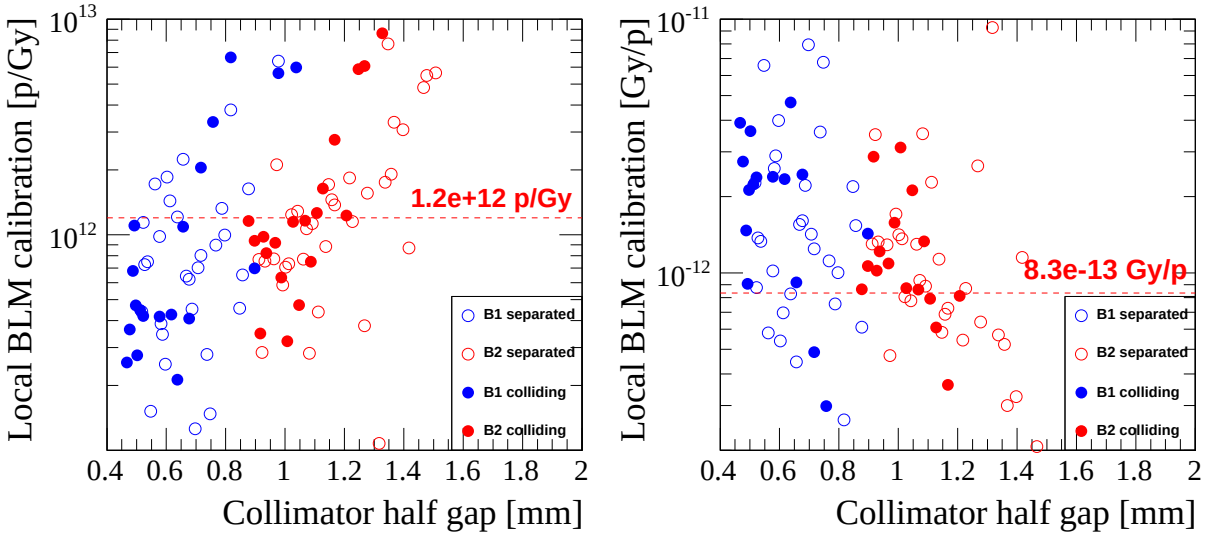

(a) Calibration factors (p/Gy)

(b) Calibration factors (Gy/p)

Figure 9: The calibration factors calculated for each loss spike in units of p/Gy (left) and Gy/p (right), as a function of the collimator half gap in mm. The red dotted line indicates the calibration factor found in the 2011 scraping MD for reference.

4.2 Evolution of beam emittance

The initial emittances are calculated from the wire-scan (see Table 4) and the synchrotron-light data. As expected, the beam emittance is reduced during the beam scraping. This is measured both by the wire scans and the synchrotron-light monitor (Fig. 10). The emittances measured at the start of the MD (2012-06-22 06:08:00) are used to convert the collimator gaps into beam sigmas. The statistical uncertainty is calculated from the difference between inward and outward wire movement. The average of the synchrotron-light measurements is used, with a statistical uncertainty deduced from the spread in data points. The final emittance value is obtained by averaging wire scan and synchrotron-light data. Its error is the combination in quadrature of the statistical errors plus a systematic error due to the difference between the two techniques. Results are reported in Table 5. The beam sizes at the collimators calculated from the initial emittances are 0.156 mm (B1 vertical) and 0.270 mm (B2 horizontal). The emittance growth rates $\gamma = \dot{\epsilon}/\epsilon$ are deduced from the slope of the synchrotron-light data before 2012-06-22 06:08:00. The expected slope of the diffusion coefficient can then be calculated as $D' = dD/dJ = \dot{\epsilon}$ (geometrical emittance). These numbers are also presented in Table 5.

Table 4: Normalized, 1σ wire-scan emittances.

Time	ϵ_x^{B1} [μm]	ϵ_y^{B1} [μm]	ϵ_x^{B2} [μm]	ϵ_y^{B2} [μm]	Notes
05:53	1.92	1.36	1.69	1.73	Non-colliding beams before scraping
06:47	1.80	1.23	1.20	1.21	Non-colliding beams after scraping
07:01	1.71	1.45	1.28	1.26	Colliding beams before scraping

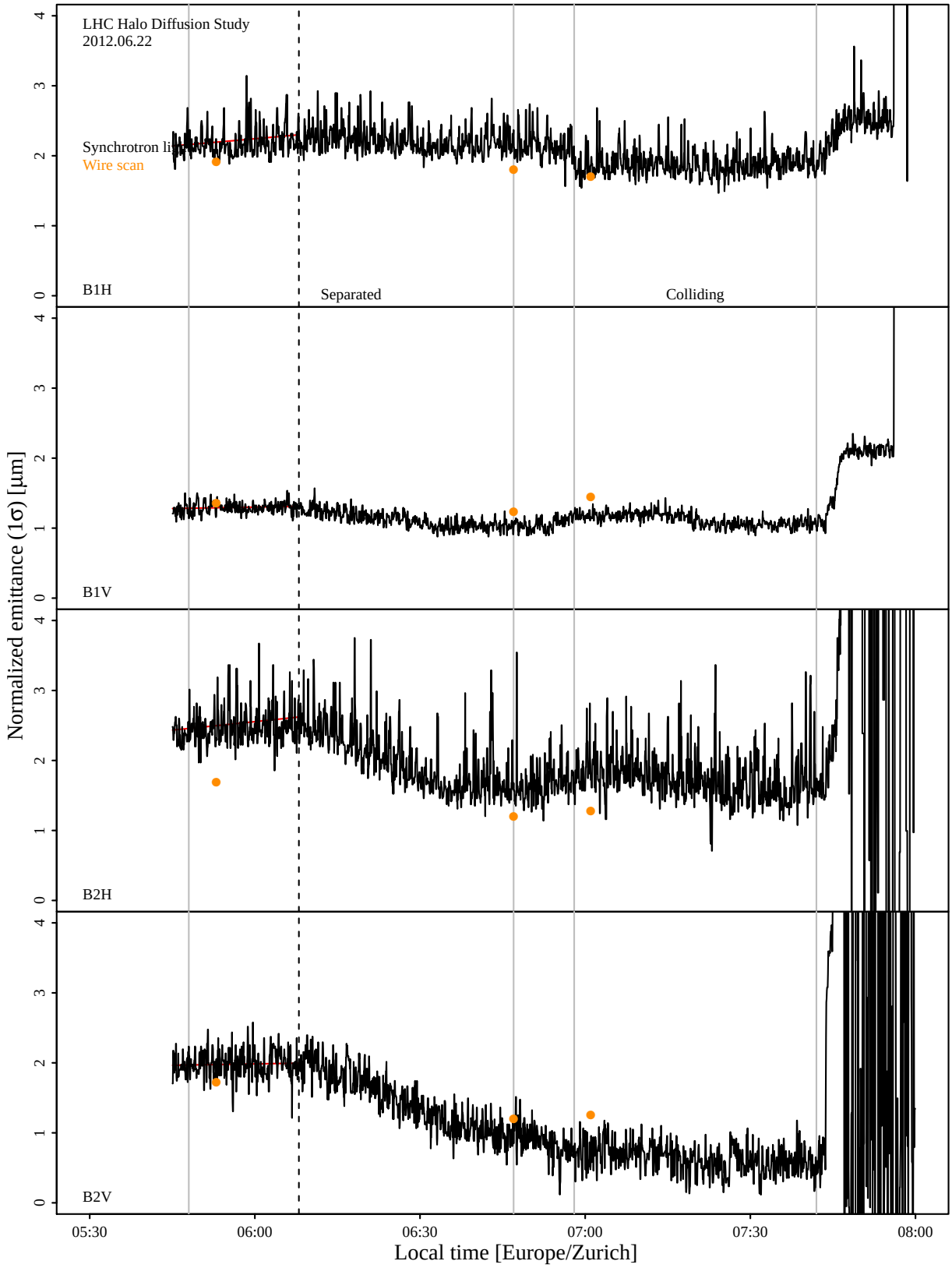

Figure 10: Synchrotron-light and wire-scan emittances over the course of the study.

Table 5: Initial emittances (wire scan, synchrotron light, average), emittance growth rates (EGR) γ, and core diffusion slopes D'.

Plane	Emittance [μm]						EGR [1/s]		Diffusion [μm/s]	
	ϵ_{ws}	$\delta\epsilon_{ws}$	ϵ_{sl}	$\delta\epsilon_{ws}$	ϵ	$\delta\epsilon$	γ	$\delta\gamma$	D'	$\delta D'$
B1 H	1.92	1.3e-02	2.15	9.6e-03	2.03	0.07	5.23e-05	1.50e-05	2.49e-08	7.4e-09
B1 V	1.36	2.0e-03	1.29	4.7e-03	1.33	0.02	1.70e-05	1.00e-05	5.27e-09	3.2e-09
B2 H	1.69	6.6e-03	2.43	1.3e-02	2.06	0.21	5.37e-05	1.90e-05	2.60e-08	9.6e-09
B2 V	1.73	4.6e-02	1.98	1.2e-02	1.85	0.09	1.10e-05	1.70e-05	4.79e-09	7.2e-09

4.3 Parametric fits of the diffusion model

The model described in Section II is used to perform fits to the inward and outward jaw movements separately. The initial values for the fit parameters are determined as follows. The steady-state rates are evaluated by averaging the losses before the step (−0.5 s from the step or earlier) and after (4 s later). The starting point for the diffusion coefficient is the value obtained from the decay 3 s after the step (where the losses are $\approx 1/\sqrt{t}$). The time of the step, t_0, is known from the time stamps of the collimator position (with 1 s resolution) and from the increase in the losses (80 ms resolution). The duration of the step Δt is estimated from the step size and the nominal jaw speed, 2 mm/s. Step time and duration can also be left as free parameters within some reasonable limits.

The distribution of the response variable (loss rate) is not Gaussian, as one can see for instance from Fig. 4, because of effects such as beam jitter and mechanical vibrations, and because of the Poissonian nature of the shower process. For this reason, fit parameters are determined by minimizing not a χ^2, but the sum of absolute deviations of the model from the data (robust estimation). For the same reason, a first estimate of the statistical errors comes from the Hessian matrix of the χ^2 function, but the final error analysis is done by bootstrapping. For each step, bootstrapping is done by resampling the data points with replacement and repeating the fit 3 times with the same initial parameters. The final results are the median of the fit results and the uncertainties come from their spread.

5 Results

Examples of the fit results are plotted in Fig. 11 (inward jaw movement) and Fig. 12 (outward jaw movement). Not all fits converged during this preliminary analysis, with the loss decay in these cases being slower than expected. Moreover, in some cases, the model cannot explain the first few seconds of losses after the step. This seems to be due to the losses decaying differently from $1/\sqrt{t}$, as shown in the first column of the plots in Fig. 11. This fact could be a combination of instrumental effects (the details of the collimator movement) and pure beam removal/cleaning. But in general, the model seems to reproduce the main features of the loss evolution with time quite well. Less data is available for the outward movement, as the losses were found to quickly decrease to the background level when a half gap of 2.2 σ for B1 and 2.8 σ for B2 was reached. This indicates a very low diffusion rate in the LHC.

The diffusion coefficients as a function of action are shown in Fig. 13 for all 4 cases: horizontal and vertical, separated and colliding beams. In the horizontal plane, there seems

to be little difference between the separated and colliding cases. In the vertical plane, collisions enhance diffusion by about 2 orders of magnitude. A significant systematic effect are the larger diffusion rates obtained from the outward steps. They are not understood, but are probably due to the fact that, after scraping, a different beam population is being sampled.

The grey curves in Fig. 13 are not an interpolation of the data: they represent the dependence $D(J)$ that one would obtain from the core emittance growth rates (Table 5). This comparison allows one to draw several conclusions: (1) the diffusion rates measured with the collimator scan technique have reasonable values; (2) without collisions, the beam halo in the LHC diffuses almost like the core up to large amplitudes; (3) no significant dynamic aperture effects (sharp rises in diffusion rate) are observed in the amplitude range explored in these experiments (7 σ-2 σ).

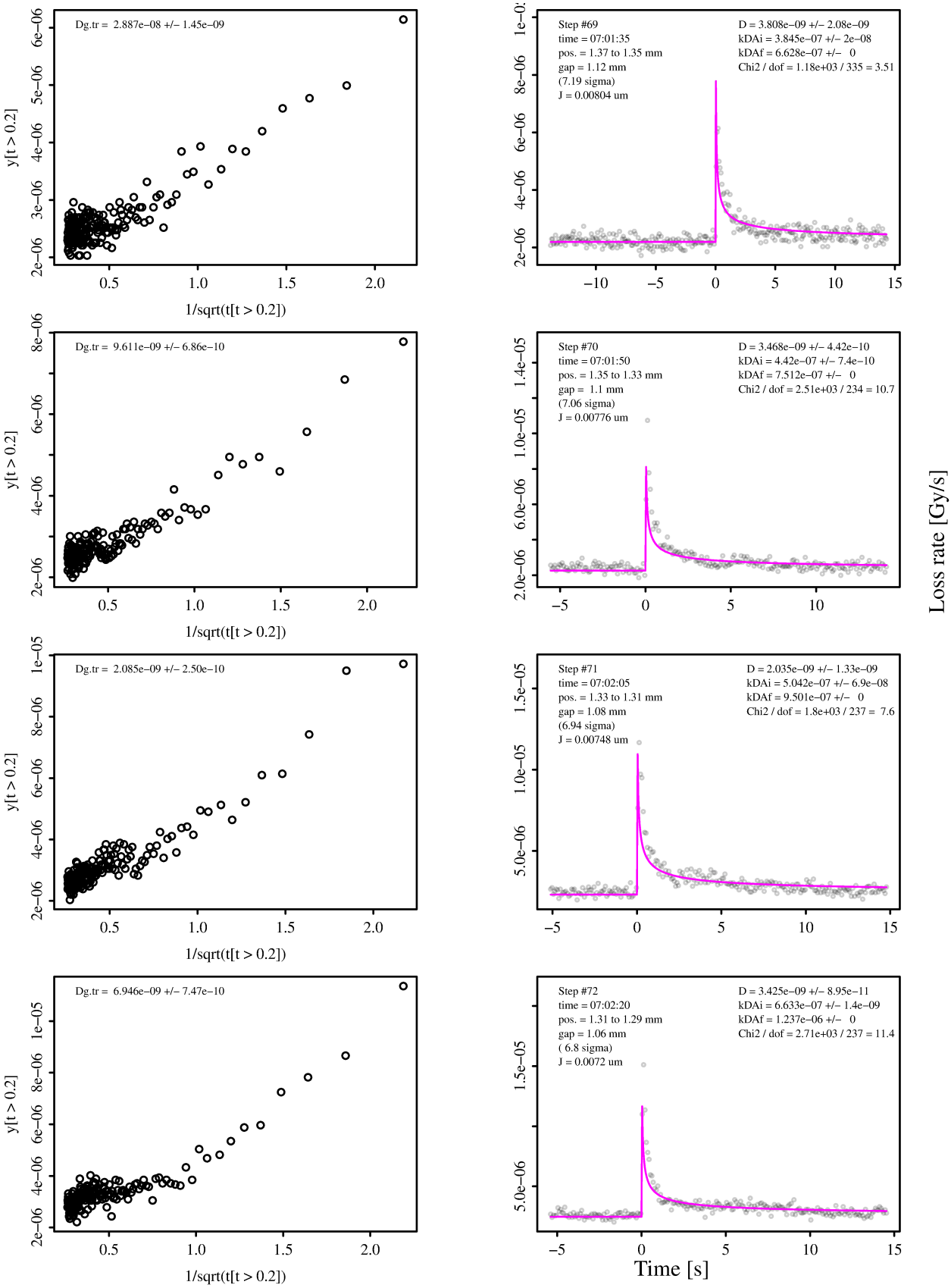

Figure 11: Examples of the loss decay part of the spike plotted as a function of $1/\sqrt{t}$ (left), a diffusion model fit to an inward step (right).

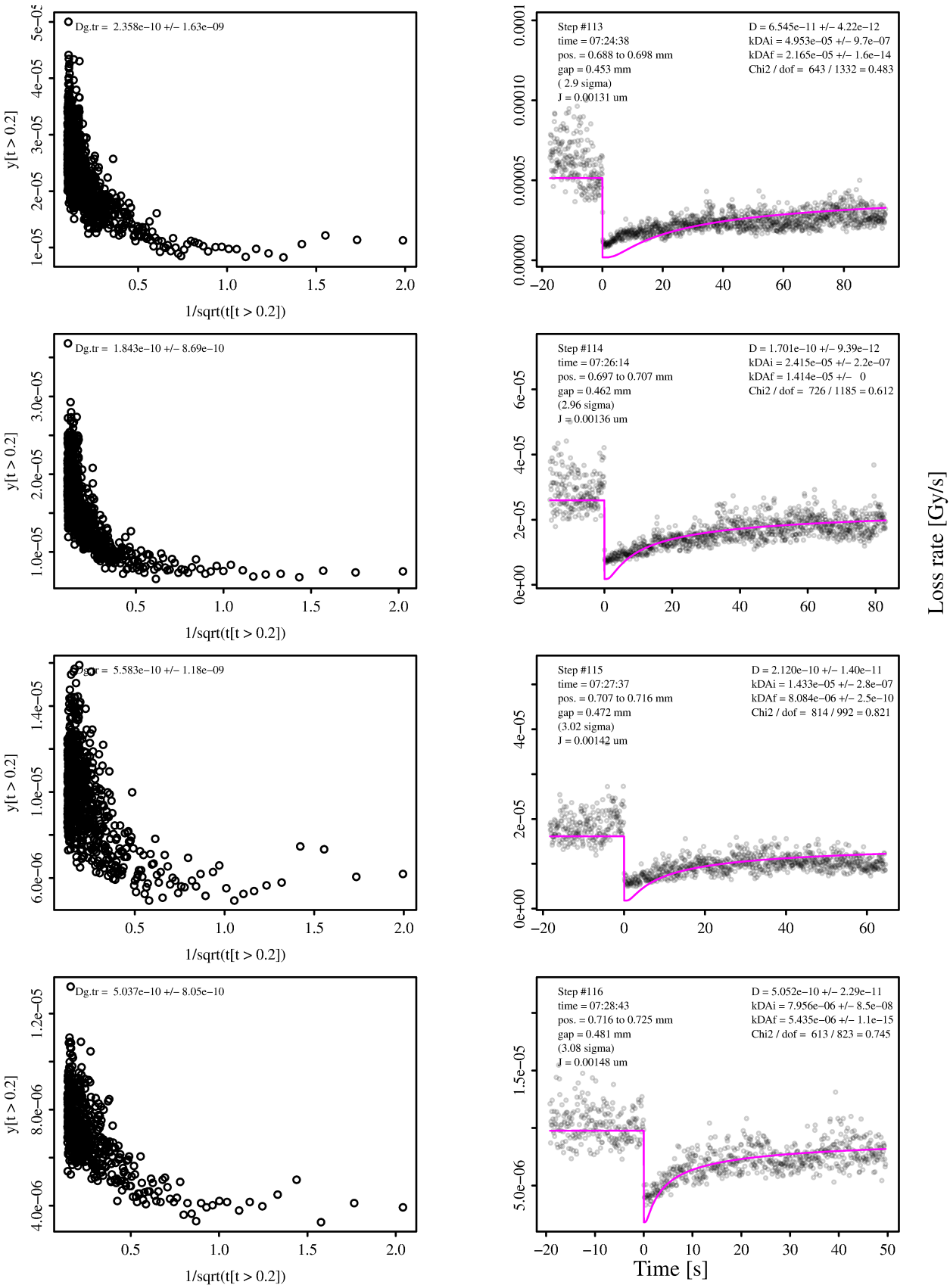

Figure 12: Examples of the loss decay part of the spike plotted as a function of $1/\sqrt{t}$ (left), a diffusion model fit to an outward step (right).

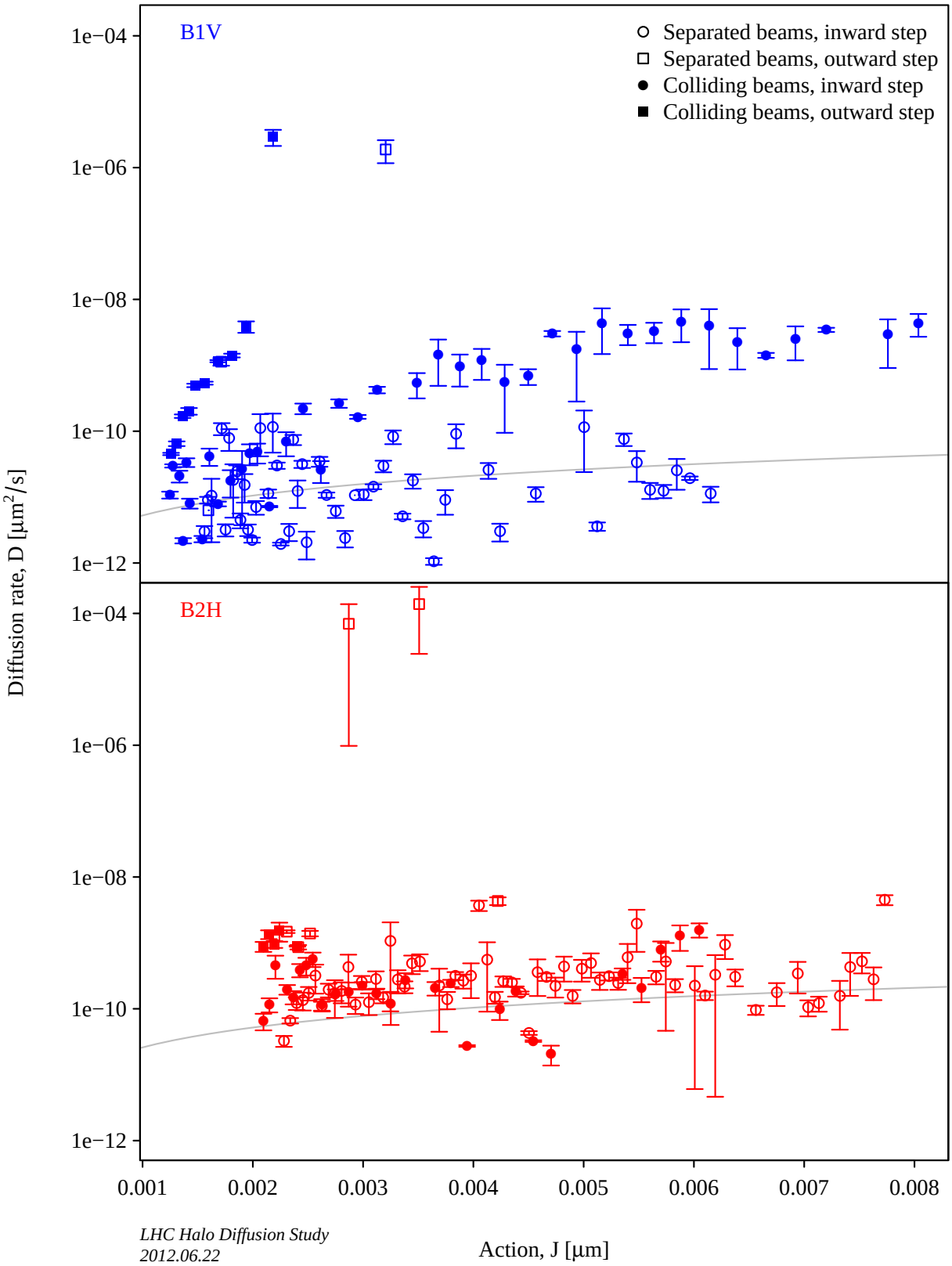

Figure 13: Diffusion coefficient as a function of action from the collimator scan (points), compared with the expectation from core emittance growth rates (lines).

6 Conclusion

This note documents the results from the first LHC beam halo scraping and diffusion study using collimators at 4 TeV. The left jaws of the TCP.D6L7.B1 (vertical plane) and TCP.C6R7.B2 (horizontal plane) were moved in steps of 5 μm to 20 μm towards the beam to obtain spikes in the BLM signal. The jaws were then retracted in steps of 20 μm to 100 μm to observe halo repopulation effects. The repopulation time was measured to be approximately a factor 3 longer than spike decay time. A diffusion model was fitted to losses observed during the jaw steps, and although it seems to reproduce the main features of the loss evolution with time quite well in both inward and outward movements, the losses during the first 3 seconds of the inward steps are more likely due to cleaning.

Acknowledgements

The authors would like to thank S. Cettour Cave, A. Macpherson, D. Jacquet and M. Solfaroli Camillocci, the LHC operators on shift during the MD. Gratitude is also expressed towards R. De Maria for providing a script to acquire the FBCT intensity data at 50 Hz.

References

[1] A. J. Lichtenberg, M. A. Lieberman. Regular and Chaotic Dynamics (Springer-Verlag, New York, 1992), p. 320.

[2] T. Chen et al. Phys. Rev. Lett. 68, 33 (1992).

[3] A. Gerasimov. Report No. FERMILAB-PUB-92-185 (1992).

[4] F. Zimmermann. Part. Accel. 49, 67 (1995); Report No. SLAC-PUB-6634 (October 1994).

[5] T. Sen, J. A. Ellison. Phys. Rev. Lett. 77, 1051 (1996).

[6] G. Valentino, R. W. Assmann, R. Bruce, S. Redaelli, A. Rossi, N. Sammut, D. Wollmann. Semiautomatic beam-based LHC collimator alignment. Phys. Rev. ST Accel. Beams 15, 051002 (2012).

[7] F. Burkart, R. W. Assmann, R. Bruce, M. Cauchi, D. Deboy, L. Lari, S. Redaelli, A. Rossi, G. Valentino, D. Wollmann. Halo scrapings with collimators in the LHC. In Proceedings of the 2nd International Particle Accelerator Conference, San Sebastian, Spain (2011).

[8] G. Stancari, G. Annala, T. R. Johnson, D. A. Still, A. Valishev. Measurements of transverse beam diffusion rates in the Fermilab Tevatron collider. In Proceedings of the 2nd International Particle Accelerator Conference, San Sebastian, Spain (2011).

[9] G. Stancari. Diffusion model for the time evolution of particle loss rates in collimator scans: a method for measuring stochastic transverse beam dynamics in circular accelerators. FERMILAB-FN-0926-APC, arXiv:1109.5010v3

[10] K.-H. Mess, M. Seidel. Collimators as diagnostic tools in the proton machine of HERA. Nucl. Instr. and Meth. in Phys. Res. A 351 (1994) 279-285.

[11] F. Burkart. Beam Loss and Beam Shape at the LHC Collimators. CERN-THESIS-2012-046 (2012).